Easy-cone state mediating the spin reorientation in the topological kagome magnet Fe3Sn2

Lilian Prodan, Donald M. Evans, Aleksandr S. Sukhanov, S. E. Nikitin, Alexander A. Tsirlin, Lukas Puntigam, Marein C. Rahn, Liviu Chioncel, Vladimir Tsurkan, István Kézsmárki

Angaben zur Veröffentlichung / Publication details:

Prodan, Lilian, Donald M. Evans, Aleksandr S. Sukhanov, S. E. Nikitin, Alexander A. Tsirlin, Lukas Puntigam, Marein C. Rahn, Liviu Chioncel, Vladimir Tsurkan, and István Kézsmárki. 2025. "Easy-cone state mediating the spin reorientation in the topological kagome magnet Fe3Sn2." *Physical Review B* 111 (18): 184442. https://doi.org/10.1103/physrevb.111.184442.

Easy-cone state mediating the spin reorientation in the topological kagome magnet Fe_3Sn_2

L. Prodan,[1,*] D. M. Evans,[1,2] A. S. Sukhanov,[3] S. E. Nikitin,[4] A. A. Tsirlin,[5] L. Puntigam,[1] M. C. Rahn,[3] L. Chioncel,[6] V. Tsurkan,[1,7] and I. Kézsmárki[1]

[1]*Experimentalphysik V, Center for Electronic Correlations and Magnetism, Institute of Physics, University of Augsburg, D-86159 Augsburg, Germany*
[2]*Department of Sustainable Energy Technology, SINTEF Industry, Oslo, Norway*
[3]*Experimentalphysik VI, Center for Electronic Correlations and Magnetism, Institute of Physics, University of Augsburg, D-86159 Augsburg, Germany*
[4]*PSI Center for Neutron and Muon Sciences, Paul Scherrer Institut, CH-5232 Villigen-PSI, Switzerland*
[5]*Felix Bloch Institute for Solid-State Physics, Leipzig University, D-04103 Leipzig, Germany*
[6]*Theoretische Physik III, Institute of Physics, University of Augsburg, D-86135 Augsburg, Germany*
[7]*Institute of Applied Physics, Moldova State University, MD-2028 ChiŞinău, R. Moldova*

(Received 3 February 2025; revised 30 April 2025; accepted 6 May 2025; published 30 May 2025)

We investigated temperature-driven spin reorientation (SR) in the itinerant kagome magnet Fe_3Sn_2 using high-resolution synchrotron x-ray diffraction, neutron diffraction, magnetometry, and magnetic force microscopy (MFM), further supported by phenomenological analysis. Our study reveals a crossover from the state with easy-plane anisotropy to the high-temperature state with uniaxial easy-axis anisotropy taking place between ∼40 and 130 K through an intermediate easy-cone (or tilted spin) state. This state, induced by the interplay between the anisotropy constants K_1 and K_2, is clearly manifested in the thermal evolution of the magnetic structure factor, which reveals a gradual change of the SR angle θ between 40 and 130 K. We also found that the SR is accompanied by a magnetoelastic effect. Zero-field MFM images across the SR range show a transformation in surface magnetic patterns from a dendritic structure at 120 K to domain-wall-dominated MFM contrast at 40 K. Our analysis suggests that the SR and associated microstructural transformations are the results of competing first- and second-order anisotropy constants.

DOI: 10.1103/PhysRevB.111.184442

I. INTRODUCTION

In anisotropic magnetic materials, the easy axis of magnetization denotes the direction along which magnetic moments align, minimizing the internal energy of the system [1]. The interplay between magnetocrystalline anisotropy, dipolar, and Dzyaloshinskii-Moriya interactions (DMI) might lead to a reorientation of magnetic moments [2,3]. The possibility of controlling magnetic degrees of freedom through the interplay between different types of interactions has been the focus of extensive studies in recent decades [4–7]. This has been extensively studied for thin films and multilayered structures where long-range magnetic dipolar interaction dominates, forcing magnetic moments to follow shape anisotropy [8]. On the other hand, in RE-TM magnets (RE = Pr, Nd, Gd, Tb, Dy, and Ho; TM = Mn, Fe, and Co) the competition between the anisotropies of rare-earth and transition-metal sublattices drives the so-called spin reorientation (SR) transition [9–12], where the direction of the easy axis of magnetization rotates from one crystallographic axis to another with varying the temperature. Moreover, temperature-induced changes in the local environment and magnetic interactions between ions at different Wyckoff positions due to symmetry change can also induce spin reorientation effects [13].

Depending on whether the easy axis shifts abruptly or rotates continuously between crystal symmetry axes, the reorientation is characterized as a first- or second-order phase transition, respectively, or can even be a smooth crossover [14]. A first-order magnetic transition is usually accompanied by a hysteresis in the magnetization and substantial changes in the magnetic entropy [15–17]. In contrast, second-order phase transitions can be traced as distinct anomalies in the magnetic susceptibility, while crossovers may not be accompanied by any sharp anomaly in thermodynamic quantities [15,18,19].

Recently, there has been growing interest in materials exhibiting SR, where the orientation of the easy axis can be influenced by a range of intrinsic and extrinsic factors, including chemical composition [20,21], shape [8], magnetic field [22–24], external pressure [25,26], strain [27,28], and light [29,30]. These factors often involve significant changes in the magnetic and electronic properties of materials and lead to the emergence of novel quantum phenomena. In particular, in several noncentrosymmetric magnets, it has been demonstrated that the interplay between DMI and magnetic anisotropy is crucial for stabilizing topologically protected (anti)skyrmion states [5,21,31–37]. Lorentz force microscopy studies on $Nd_2Fe_{14}B$ have revealed the formation of magnetic bubbles with zero topological number and magnetic

*Contact author: lilian.prodan@uni-a.de

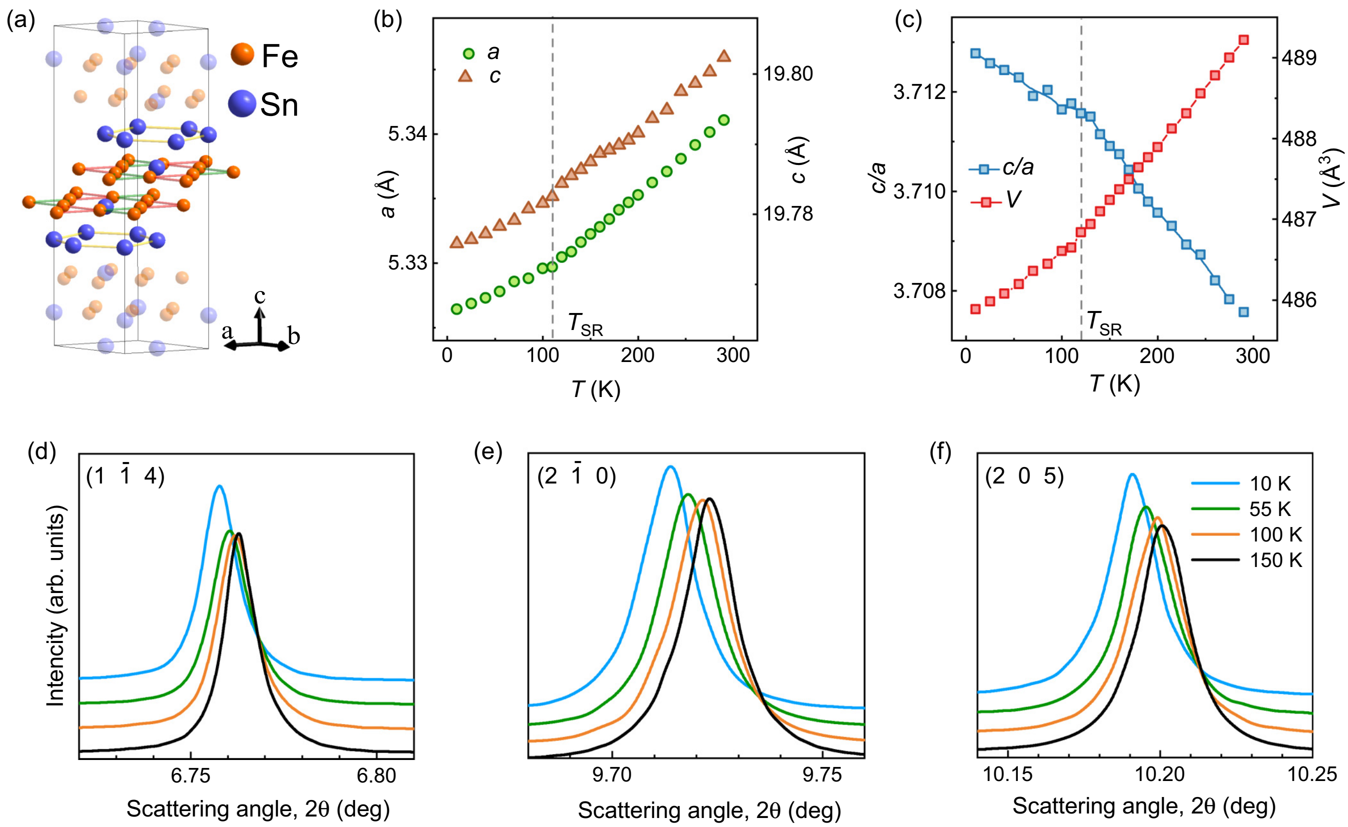

FIG. 1. Crystal structure and high-resolution powder x-ray synchrotron diffraction for Fe_3Sn_2. (a) Schematic representation of the rhombohedral $R\bar{3}m$ crystal structure [45]. (b) Temperature dependence of the lattice parameters a and c. (c) Temperature variation of the ratio c/a and the unit-cell volume. The vertical dashed lines in panels (b) and (c) indicate the changes in the slope at the spin-reorientation temperature T_{SR}. (d)–(f) Experimental profiles of the $(1\bar{1}4)$, $(2\bar{1}0)$, and (205) Bragg reflections as measured at different temperatures by high-resolution synchrotron powder XRD. The same color code is used in panels (d)–(f).

skyrmions induced by SR [38]. Moreover, the enhancement of magnetoresistance, topological, and anomalous Hall effects have been reported near the SR transition in various two-dimensional van der Waals magnets [7,39,40], rare-earth topological kagome magnets of RMn_6Sn_6-type [41,42], and Heusler magnets [43]. These phenomena are attributed to changes in Berry curvature caused by spin reorientation [44].

Here, we investigate the SR effect in the itinerant kagome magnet Fe_3Sn_2. The crystal structure consists of bilayers of Fe_3Sn kagome networks separated by hexagonal Sn layers and stacked along the $\boldsymbol{c}$ axis [see Fig. 1(a)], corresponding to the rhombohedral $R\bar{3}m$ space group [45]. Fe_3Sn_2 is ferromagnetic below 650 K and its magnetic anisotropy is reported to change from the easy axis above 250 K to the easy plane below 60 K [46–49]. This material has recently attracted much attention as a host for massive Dirac fermionic states [50], Weyl nodes [51], topological flat bands [52], and helical nodal lines [53]. The interplay between the electronic band topology and magnetism gives rise to prominent phenomena, including large anomalous and topological Hall effects [50,54], magneto-optical effects [51,53], and topologically protected skyrmionic bubbles [55,56]. Moreover, recent advancements in the field have suggested that Fe_3Sn_2 manifests anomalous charge carrier behavior and strong orbital contribution to the magnetism and transport properties [57–60].

Despite intense studies using various measurement techniques such as magnetization, ac susceptibility, neutron diffraction, magnetic force microscopy (MFM) [61–65], optical spectroscopy [51], Raman scattering [49,64], and magnetotransport measurements [66–68], the mechanism of spin reorientation in Fe_3Sn_2 remains unclear. Specifically, whether the transition is gradual or abrupt, its origin and its impact on the magnetic domain configuration are still debated. Given that the interplay between topologically nontrivial band structure and magnetization is expected to play a crucial role in the electronic response in Fe_3Sn_2 [69–71], it is essential to clarify the origin of the SR and understand the accompanying variations in spin texture with temperature and magnetic field.

In this study, we investigated the temperature-driven SR in the topological kagome ferromagnet Fe_3Sn_2 through a combination of experimental techniques and phenomenological analysis. The temperature dependence of the anisotropy constants K_1 and K_2, the evolution of the magnetic structure factor $\mathbf{M_Q}(T)$, and MFM imaging indicate that the high-temperature state, with uniaxial easy-axis anisotropy, transforms to a mixed state before developing an in-plane magnetization state at low temperatures, consistent with easy-plane anisotropy. This transformation is characterized by a gradual change of the angle θ spanned by the magnetization and the c axis, taking place between ≈40 and 130 K. The zero-field MFM images across the SR range show strong variation in magnetic contrast. Phenomenological analysis suggests that the SR and associated microstructural transformations are caused by competing anisotropy constants K_1 and K_2.

II. EXPERIMENTAL DETAILS

Single crystals of Fe_3Sn_2 have been grown by the chemical transport reaction method using preliminary synthesized polycrystalline material and iodine as a transport agent. The growth was carried out in a two-zone horizontal furnace in a temperature range between 670 and 740 °C. Shiny hexagonal crystals with dimensions up to 4 mm along the largest side were obtained in the hot part of the ampule. The chemical composition of the samples was checked by energy-dispersive x-ray spectroscopy analysis utilizing the ZEISS Crossbeam 550 system.

High-resolution x-ray diffraction (XRD) data were collected on the polycrystalline sample of Fe_3Sn_2. The measurements were performed in the transmission geometry of the ID22 beamline at the European Synchrotron Radiation Facility (ESRF, Grenoble, France) using the multianalyzer setup [72,73]. The wavelength of 0.354 32 Å was calibrated with a silicon standard (NIST, 640c). The sample temperature was stabilized with the liquid-helium-cooled cryostat. To reduce the effect of beam heating, the capillary was kept open at one end and exposed to the helium-flow atmosphere. The Rietveld refinement was performed using the JANA2006 program [74].

Magnetic properties were studied with the SQUID magnetometer (MPMS 3, Quantum Design) in the temperature range of 2–400 K and magnetic fields up to 7 T.

Neutron diffraction data were collected on the EIGER triple-axis instrument (PSI, Switzerland) with a neutron wavelength of 2.36 Å [75]. A few single crystals were coaligned to increase the total sample mass. The backscattering Laue x-ray showed that the relative misalignment between the individual crystals does not exceed 1 deg. The sample was inserted into the cryostat by its vertical [100] axis, placing the reciprocal (HHL) plane in the horizontal scattering plane. A graphite filter was placed after the sample to suppress the higher-order harmonics.

To investigate the magnetic domain textures of Fe_3Sn_2, we perform MFM on an attocube attoAFM I, equipped with a superconducting magnet, and cooled by a liquid-helium cryostat. The sample environment has ca. 150 mbar of He as an exchange gas. PPP-MFMR nanosensor probes were used; these have a hard magnetic coating and a radius of curvature of $\leqslant$50 nm. Once each temperature was reached, the equipment was allowed to thermalize for about an hour to ensure full thermal equilibrium. Data were collected in a single pass with the tip lifted 200 nm above the defined contact point, and the pixel size is 20 nm. The images show changes in frequency, recorded via a phase-sensitive feedback loop, and, as usual, the image contrast is proportional to the gradient of the stray magnetic field at the tip [76].

III. RESULTS AND DISCUSSION

Figures 1(b) and 1(c) show the structural parameters derived from the Rietveld refinement of the XRD data between 300 and 10 K. The cell parameter a decreases by ∼3%, while c decreases by ∼2% [see Fig. 1(b)]. Both parameters exhibit a change in the slope below 120 K, which is also reflected in the temperature evolution of the c/a ratio and the unit-cell volume V, Fig. 1(c), indicating a magnetoelastic response to the spin reorientation. Importantly, the reflection width changes only marginally between 300 and 10 K, and none of the reflections splits on cooling [see Figs. 1(d) and 1(e)]. Therefore, no deviation from the trigonal symmetry is observed down to the lowest measured temperatures.

Recent studies of Mn_3Sn and Fe_3Ge kagome magnets and two-dimensional Fe_4GeTe_2 have also reported slight changes in structural parameters, such as the lattice constants a and c, the c/a ratio, and the unit cell volume V at the spin reorientation [77–79]. These changes were attributed to thermal expansion of the lattice and may contribute to variations in magnetic anisotropy, thereby driving the spin reorientation [80].

Figures 2(a) and 2(b) show the isothermal magnetization curves of Fe_3Sn_2 measured for magnetic fields applied in different orientations: within the ab plane, along the a axis (in-plane), and along the c axis (out-of-plane). At 2 K, full saturation of magnetization M_s along the a axis is achieved in fields of ∼0.1 T, while along the c axis, the saturation requires approximately 1 T. The M_s values calculated at 5 T are 2.09 μ_B/Fe and 2.17 μ_B/Fe for $\mathbf{H}||a$ and $\mathbf{H}||c$, respectively. With increasing temperature, the saturation field increases for $\mathbf{H}||a$ and decreases for $\mathbf{H}||c$. The initial susceptibility extracted from fields close to zero, χ_0', measured for $\mathbf{H}||a$ and $\mathbf{H}||c$ is shown in Fig. 2(c).

The temperature-dependent magnetization for $\mathbf{H}||a$ was measured in various fields and using various cooling protocols. Figure 2(d) shows a continuous increase of magnetization as the temperature decreases to 60 K, saturating below this temperature. Unlike the findings in Ref. [63], our data show gradual variation with temperature without abrupt changes between 400 and 2 K. The zero field-cooled magnetization and field-cooled magnetization measurements display only minor hysteresis, which can be likely attributed to the dynamics of magnetic microstructures described later.

Next, we discuss the uniaxial crystal anisotropy energy density (E_A) that for the hexagonal system is usually expressed as a power series of the form [81]

$$E_A = \sum_n K_n \sin^{2n}\theta \ . \tag{1}$$

Here, K_n is the uniaxial anisotropy constant of order n and θ is the angle between M and the c axis. In particular, in a rhombohedral system, the c axis is the axis of threefold rotational symmetry, and the total energy density is expressed as

$$E_A = K_1 \sin^2\theta + K_2 \sin^4\theta + K_3 \cos\theta \sin^3\theta \cos 3\phi, \tag{2}$$

where the angle ϕ is the azimuthal angle in the ab plane.

The anisotropy energy minimization in the presence of an external applied field provides the equilibrium direction of magnetization. In the limit of zero external field, the total anisotropy energy is mainly determined by $K_u \approx K_1 + K_2$. This K_u constant can be estimated directly from the experimental data as the difference between the energy necessary

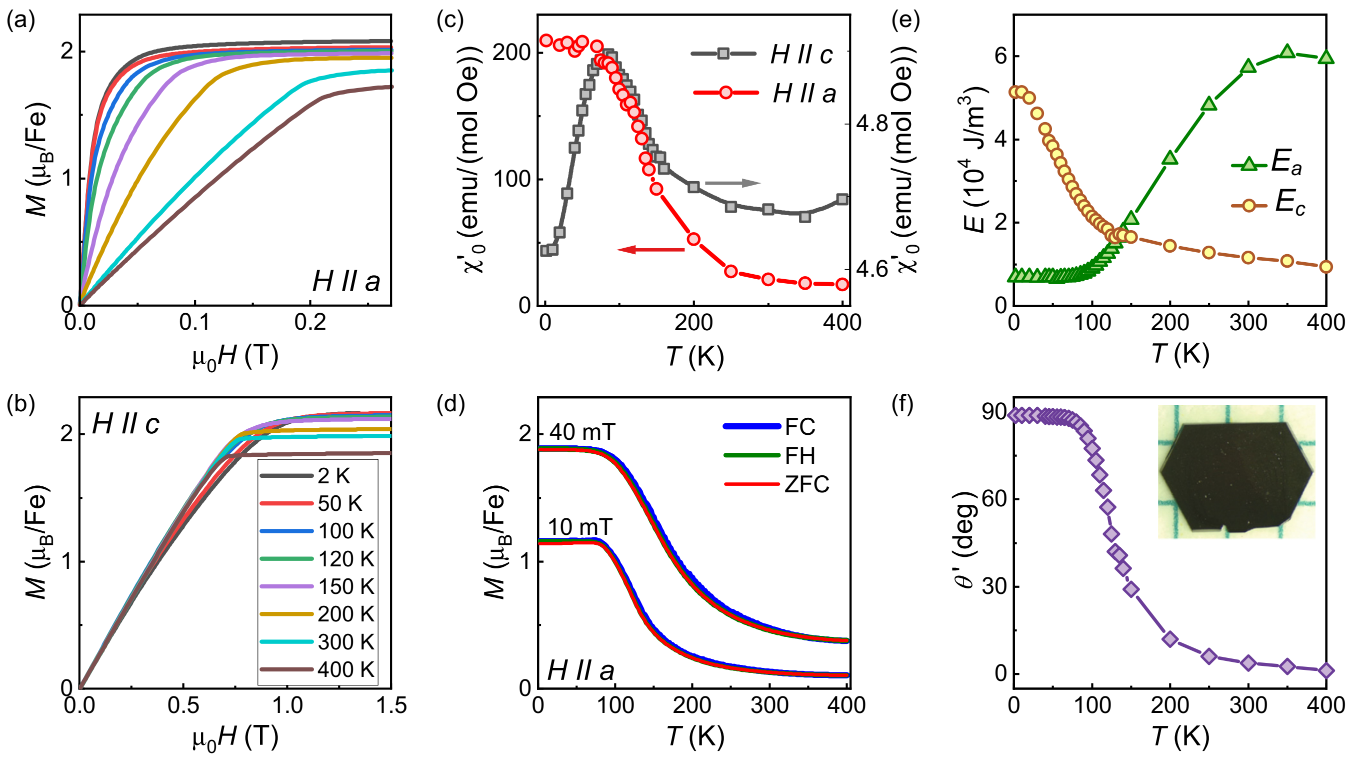

FIG. 2. SQUID magnetometry data of ferromagnetic Fe_3Sn_2. (a) Magnetization curves vs magnetic field applied along the *a* axis and (b) along the *c* axis, respectively. (c) Temperature dependence of differential magnetic susceptibility extracted from zero-magnetic-field measurements for $\mathbf{H}||a$ and $\mathbf{H}||c$. (d) Zero-field-cooled (ZFC), field-cooled (FC), and field-heated (FH) magnetization as a function of the temperature measured in fields of 10 and 40 mT applied along the *a* axis. (e) The temperature dependence of energy of magnetization for E_a and E_c used for calculating the uniaxial anisotropy constant K_u. (f) The temperature dependence of the spin reorientation angle θ' calculated from the magnetization in $H_i = 5$ Oe. The inset of panel (f) includes an optical image of the *ab* plane of the as-grown Fe_3Sn_2 crystal on a millimeter scale.

to saturate the magnetization along the two orthogonal directions:

$$K_u = E_a - E_c = \int_0^{M_s^a} H_i\, dM_a - \int_0^{M_s^c} H_i\, dM_c. \quad (3)$$

This approach known as the *"area method"* [82] has been applied previously, e.g., for the easy-plane kagome ferromagnet Fe_3Sn [83].

Figure 2(e) presents the temperature dependence of the energies E_a and E_c used to calculate the uniaxial anisotropy constant K_u. Here, the magnetization was corrected for the demagnetization factor, $H_i = H - DM$, where H is the applied external magnetic field, D represents the demagnetization coefficient, and M is the magnetization. The effect of demagnetization on the magnetization curves measured for different directions is shown in Fig. 6. E_a decreases with a decrease in temperature, while E_c increases, reflecting the change of the anisotropy. At 120 K, the integrals have equal values, indicating that the same energy is required to align the magnetic moment along the *a* or *c* axes. Consequently, $K_u = 0$ at this temperature [see Fig. 3(a)]. At temperatures below 120 K, K_u is negative, reaching -35 kJ/m^3 at 2 K, while at temperatures above 120 K, K_u is positive and reaches 57 kJ/m^3 at 400 K. The calculated K_3 constant is $\sim$1 kJ/m^3 at 2 K, indicating negligible basal plane anisotropy in Fe_3Sn_2. The latter is further supported by the absence of a 60° periodicity in the angular dependence of the magnetization within the *ab* plane.

Figure 3(a) shows the temperature dependence of the anisotropy constants K_u, K_1, and K_2. In the temperature range where the orientation of moments is well-defined, we also calculated K_1 and K_2 independently by the Sucksmith-Thompson (S-T) method fitting the S-T isotherms $M/H = f(M^2)$ [84]. At 2 K, K_1 is negative (easy-plane anisotropy) and reaches ~ -75 kJ/m^3 [see Fig. 3(a)]. At high temperatures, K_1 is positive (easy-axis anisotropy) and reaches $\sim$55 kJ/m^3 at 400 K. In contrast, K_2 remains positive throughout the whole temperature range. At 2 K, K_2 has a value $\sim$30 kJ/m^3. These values are in agreement with the results reported in Ref. [62]. However, at the intermediate temperatures, 50 K $\leqslant T \leqslant$ 150 K, the S-T isotherms show strong nonlinearity and this method gives nonreliable values of anisotropy constants.

In the following, we present an approach for extracting anisotropy constants when the S-T isotherms become nonlinear. The minimization of magnetic free energy described in Eq. (1), with respect to the reorientation angle θ (being the order parameter), gives the equilibrium configuration. In this case, the relation between the zero-field differential susceptibility for $\mathbf{H}||c$ and the anisotropy constants, the saturation magnetization for $\mathbf{H}||c$, and the demagnetization has the

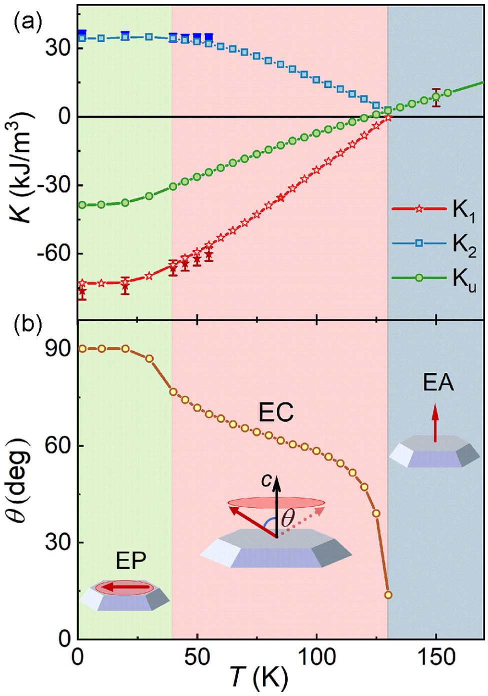

FIG. 3. (a) Temperature dependence of the anisotropy constants K_u, K_1, and K_2 obtained by the area method and Eq. (4) (open symbols). The closed symbols show K_1 and K_2 obtained by the Sucksmith-Thompson method. (b) Temperature dependence of the spin reorientation angle θ, as calculated using K_1 and K_2. The insets show schematically the spin arrangement in easy-plane (EP), easy-cone (EC), and easy-axis (EA) states.

following form (see Appendix A):

$$\chi(T) = \frac{M_s^2(T)}{D M_s^2(T) - 2(K_1 + 2K_2)}. \quad (4)$$

The resulting temperature dependence of K_1 and K_2 is shown in Fig. 3(a). Below 50 K, the values of K_1 and K_2 agree well with those obtained by the S-T method, corroborating the data obtained through our approach. Considering the small contribution of $K_3 \cos\theta \sin^3\theta \cos 3\phi$ to the total energy density, including such a term will act as a small correction to the Eq. (4) (see Appendix B).

When K_3 is negligibly small, there is no preferred azimuthal direction, suggesting that the magnetic spin structure can adopt an easy-cone state with degenerate orientations around the c axis. In this scenario, the interplay between K_1 and K_2 governs the transition from the easy-axis (EA) to the easy-plane (EP) state via the easy-cone (EC) state [82,85]. In the EC state, the easy direction of the magnetization is tilted away from both the hexagonal axis and the hexagonal plane, i.e., $0 < \theta < 90^\circ$, and the rotation angle is defined by $\theta(T) = \arcsin\sqrt{-K_1/2K_2}$ [11]. Figure 3(b) shows the temperature dependence of θ, indicating that the transition from EP to EC takes place at $T_{SR1} \approx 40$ K, when the condition $-K_1 = 2K_2$ is satisfied. Upon heating in the easy-cone state, the magnetic moments rotate gradually from the a axis towards the c axis. At $T_{SR2} \approx 130$ K, K_1 changes sign, defining the transition to

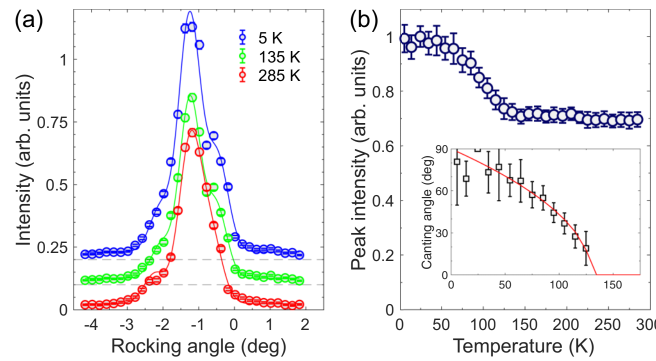

FIG. 4. Neutron diffraction. (a) The rocking-scan intensity of the (003) Bragg peak at different temperatures. The data were offset for clarity by the dashed lines. (b) The temperature dependence of the integrated intensity (area) of the (003) Bragg peak. The inset shows the calculated spin reorientation angle θ. The red curve is a guide to an eye.

the easy-axis state. Such a transition at T_{SR1} and T_{SR2} is of a second order [85].

The angle of SR was additionally calculated from the ratio of low-field magnetization for $\mathbf{H}||a$ and $\mathbf{H}||c$ for the internal magnetic field $H_i = 5$ Oe using the relation $\theta' = \arctan(M_a/M_c)$ [see Fig. 2(f)]. The calculated θ' also shows gradual decrease with increasing temperature, being in qualitative agreement with our magnetization and the Mössbauer studies [48].

For an independent quantification of the SR angle, we performed single-crystal neutron diffraction experiments. According to the neutron polarization factor, the scattering intensity vanishes when the neutron momentum transfer $\mathbf{Q}$ aligns with the magnetic structure factor $\mathbf{M_Q}$. Therefore, it is convenient to track the in-plane projection of the spin upon its canting by the intensity of the allowed Bragg peaks of the indexes $(00L)$, where $L = 3, 6, 9, \ldots, 3n$. Indeed, when the spins are strictly oriented along the $\mathbf{c}$ axis, the $(00L)$ peaks contain only the nuclear intensity and no magnetic contribution. As soon as the spins deviate from the $\mathbf{c}$ axis, the $\mathbf{Q} \parallel \mathbf{M_Q}$ condition is no longer fulfilled, and a finite magnetic intensity $\propto S_{\mathbf{ab}}$ appears on top of the nuclear Bragg peaks.

Figure 4(a) shows the intensity of the Bragg peak (003) collected by rotating the crystal around its [100] at a fixed detector angle of $2\theta = 41.21^\circ$ (rocking scan). As can be seen, the measurements reveal almost identical Bragg peaks at 285 and 135 K, whereas the peak intensity significantly increases at a lower temperature of 5 K. To analyze its temperature evolution, we plotted the total intensity integrated over the rocking angle of the [003] peak in Fig. 4(b). The flat curve from room temperature down to ~130 K suggests the spins remain along the $\mathbf{c}$ axis and only the temperature-independent nuclear intensity is recorded. Below this temperature, the intensity shows a gradual increase over a wide temperature range down to ~40 K, after which it saturates. Assuming that the spins are fully in-plane at the lowest temperature and that the magnitude of the magnetic moment does not significantly change below T_{SR}, we can follow the temperature dependence of the SR by the θ angle ($\theta = 0$ when $\mathbf{M} \parallel c$) estimated from neutron diffraction, as shown in the inset of Fig. 4(b).

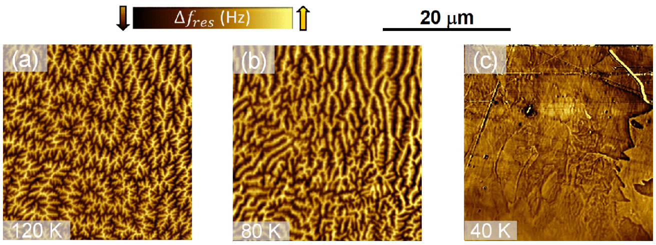

FIG. 5. Evolution of the magnetic domain patterns illustrated using MFM contrasts. Panel (a) shows dendritelike domains with an out-of-plane component of magnetization measured at 120 K. Panel (b) shows a stripe domain pattern forming at 80 K. Panel (c) illustrates the lack of out-of-plane contrast at 40 K.

This rotation of magnetic moments from the **c** axis to the *a* axis should lower the symmetry by breaking the threefold rotational symmetry for any $\theta > 0$. The fact that the symmetry lowering from the trigonal state to an orthorhombic state has not been observed by our high-resolution x-ray study may be due to (a) the weakness of the corresponding distortion and/or (b) the restoring of the trigonal symmetry in the macroscopic sense due to the coexistence of the energetically equivalent six domains of the EP state.

For an independent confirmation of the SR in our Fe_3Sn_2 single crystals, the magnetic domain patterns were imaged by MFM in zero field on the as-grown *ab* plane of the crystal shown in the inset of Fig. 2(f). Figure 5(a) shows the MFM pattern at 120 K, revealing a dendritelike fern contrast. This is similar to the domain pattern at 300 K which previous work showed to arise from magnetization pointing upward and downward along the **c** axis (see, e.g., Refs. [56,62,63]). We note that the fern pattern is caused by surface branching of the underlying domains, and therefore the domain patterns observed here with MFM in Fe_3Sn_2 do not reflect the magnetic microstructure in the bulk. Indeed, such dendritelike domain patterns have been reported to be characteristic of uniaxial easy-axis magnets [86]. With cooling down to 80 K, where the magnetic easy axis is already tilted away from the *c* axis according to our magnetometry and neutron diffraction results, the MFM contrast undergoes gradual changes, namely, the dendritelike structure transforms to a more simple stripe domain pattern. Similar transformation of magnetic domains in Fe_3Sn_2 thin plates was reported to result from tilting of spins away from the **c** axis [87]. With further cooling to 40 K, the stripe pattern vanishes. In fact, in Fig. 5(c) the magnetic contrast caused by out-of-plane stray fields disappears, indicating that the sample becomes in-plane magnetized. In that case, vortices and antivotices (also termed in-plane flux closure domains) are expected to form, as shown for the easy-plane ferromagnet Fe_3Sn [83]. These results are qualitatively in agreement with MFM results reported in Refs. [63,65] and clearly demonstrate the onset of SR from a high-temperature easy-axis state to a low-temperature easy-plane state.

A quantitative analysis of the magnetic behavior at the micrometer-length scale is usually obtained by micromagnetic simulations, which can provide a comprehensive description of MFM images. In combination with density functional theory, these simulations can consider various forms of exchange interactions and anisotropies. While here we focus on the analysis of the temperature-dependent SR process, MFM imaging is only used to provide another independent confirmation of the SR. A multiscale approach reproducing the magnetic patterns observed in zero as well as finite magnetic fields will be presented in a forthcoming work.

IV. CONCLUSION

In conclusion, we have investigated the temperature-driven spin reorientation in the topological kagome ferromagnet Fe_3Sn_2 by high-resolution synchrotron x-ray diffraction, magnetometry, neutron diffraction, and MFM techniques supported by phenomenological analysis of magnetic anisotropy. Our study reveals an intermediate easy-cone state that appears during the reorientation from the easy-plane state towards the easy-axis state. Although spin reorientation is accompanied by a weak magnetoelastic effect, no lowering of the crystal symmetry from trigonal could be resolved down to the lowest temperatures. The temperature dependence of the first- and second-order anisotropy constants, K_1 and K_2, and the evolution of the magnetic structure factor $\mathbf{M_Q}(T)$ show that the easy-cone state is stable between $T_{SR1} \approx 40$ K and $T_{SR2} \approx 130$ K. The spin reorientation angle θ, determined from the magnetometry and neutron diffraction data, exhibits a gradual change between T_{SR1} and T_{SR2}. Furthermore, zero-field MFM images across the SR range evidence a transformation in magnetic contrast, from a dendritic structure at 120 K to well-defined domain walls at 40 K, providing a direct visualization of spin reorientation in Fe_3Sn_2. Our phenomenological analysis highlights the dominant role of competition between anisotropy constants. These findings provide a clear insight into the nature and dynamics of spin reorientation in topological magnet Fe_3Sn_2, highlighting its fundamental role in the evolution of magnetic anisotropy.

ACKNOWLEDGMENTS

We thank ESRF for providing the beam time for the project HC-4369 and acknowledge Ola Grendal as well as Andrew Fitch for their technical support at ID22. This work was supported by the Deutsche Forschungsgemeinschaft (DFG, German Research Foundation) under Grant No. TRR 360–492547816. D.M.E. acknowledges and thanks the DFG for financial support via DFG Individual Fellowship No. EV 305/1-1. V.T. acknowledges support through Project ANCD (code 011201, Moldova). This work is partially based on experiments performed at the Swiss spallation neutron source SINQ, Paul Scherrer Institute, Villigen, Switzerland.

DATA AVAILABILITY

The data that support the findings of this article are openly available [73,88].

APPENDIX A: THE FORMULA OF DIFFERENTIAL SUSCEPTIBILITY

In the following we present a brief description of the derivation of Eq. (4). To simplify formulas, we introduce the reduced parameters: $k = K_1/K_2$, $A = M_sH/K_2$, and $B = DM_s^2/(2K_2)$. The free energy is a functional of applied field and temperature and contains besides the Zeeman term the demagnetization energy contribution:

$$E[k,A,B]=\frac{E-K_0}{K_2}=k\sin^2\theta+\sin^4\theta-A\cos\theta+B\cos^2\theta. \quad \text{(A1)}$$

The substitution with a variable $\gamma=\cos\ \theta=M_{||}/M_s$ leads the free energy into a fourth-order expression in γ. The equilibrium configuration for the orientation of the magnetic moments is found by minimization with respect to the reorientation angle $\theta=\arccos\gamma$. Conventionally, this angle is measured with respect to the c axis. The partial derivative with respect to γ, $\partial E[k,A,B]/\partial\gamma=0$, therefore produces a third-order equation that is analytically solvable. Two of its complex solutions are discarded, and the real solution has an analytical form:

$$\gamma=\frac{[432A+\sqrt{186624A^2+4(-48+24B-24k)^3}]^{1/3}}{12\times 2^{1/3}}-\frac{-48+24B-24k}{6\times 2^{2/3}[432A+\sqrt{186624A^2+4(-48+24B-24k)^3}]^{1/3}}.$$

The above equation represents, in fact, the reduced magnetization $M_{||}/M_s$, with $M_{||}$ being the magnetization along the applied field and M_s the saturated magnetization (as described in the main text). Accordingly, the differential susceptibility is computed as a derivative of magnetization with respect to the applied field:

$$\chi(H,T)=\frac{dM_{||}}{dH}=\frac{M_s^2}{K_2}\frac{d\gamma}{dA}. \quad \text{(A2)}$$

Within the reduced variables taking the derivative with respect to the variable A, $d\gamma/dA$, finally the limit $A\to 0$ gives

$$\chi(k,A,B)|_{A\to 0}=\frac{M_s^2}{K_2}\frac{1}{2(-2+B-k)}. \quad \text{(A3)}$$

Inserting back the forms of the reduced variables B and k leads to the form presented as Eq. (4).

APPENDIX B: THREEFOLD ANISOTROPY CORRECTIONS

In a more general framework considering also the possibility of the existence of threefold in-plane anisotropy, we derive in the following the corrections to the static susceptibility. The total energy density for a rhombohedral system reads as follows:

$$E_6[k,A,B,C]=E[k,A,B]+C\cos\theta\sin^3\theta, \quad \text{(B1)}$$

with $C=(K_3/K_2)\cos 3\phi$, where ϕ is the azimuthal angle and $E[k,A,B]$ has the form of Eq. (A1). In most cases, the (K_3) contribution is orders of magnitude smaller than K_1 and K_2. A complication in solving for the additional term of energy density constitutes the product term $\cos\theta\ (\sin\theta)^3$. We considered the decomposition of this product in terms of Legendre polynomials $[P_l(\cos\theta)]$ up to the sixth order: $(\sin\theta)^3\approx 1-\frac{3}{2}\cos^2\theta+\frac{3}{8}\cos^4\theta+\frac{1}{8}\cos^6\theta$, and we took a further simplification up to its second term. Following a similar prescription by introducing the variable γ and solving for the variable γ, the equation $\partial E[k,A,B,C]/\partial\gamma=0$ provides us a third-order equation in γ, similarly with one real and two complex solutions. For the physical (real) solution, the corresponding susceptibility is obtained in vanishing fields according to Eq. (A2). In order to reveal the correction due to the additional term proportional to C in the energy density, we further expand the susceptibility in series for small C values. As the first order cancels, the second-order correction to Eq. (A3) is

$$\chi(k,A,B,C)|_{A\to 0}\approx\chi(k,A,B)|_{A\to 0}+\frac{M_s^2}{K_2}\frac{3}{8}\frac{-4+3B-3k}{(-2+B-k)^4}C^2. \quad \text{(B2)}$$

Thus, we have shown that the threefold in-plane anisotropy addition is possible and this provides second-order correction to the static susceptibilities. However, considering the smallness of K_3, the C correction can be neglected in the case of Fe_3Sn_2.

APPENDIX C: DEMAGNETIZATION EFFECT

Figure 6 presents the experimental as-measured magnetization curves $[M(H_{ext})]$ in comparison with magnetization as a function of the internal magnetic field $[M(H_i)]$ calculated as $H_i=H-DM$. This figure demonstrates the dominant effect of demagnetization for $\mathbf{H}||c$.

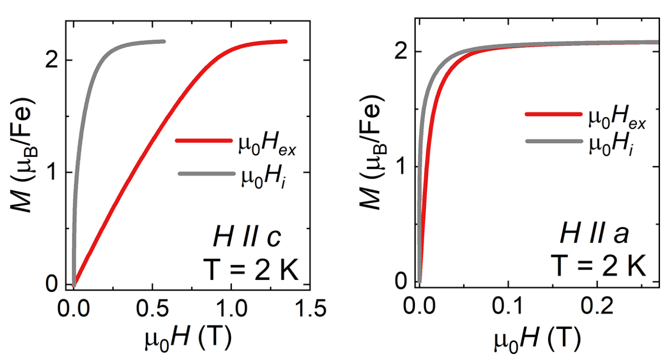

FIG. 6. Demagnetization effect on the magnetization curves of Fe_3Sn_2. $\mu_0 H_{ex}$ stands for external magnetic field and $\mu_0 H_i$ is the internal magnetic field.

[1] K. H. J. Buschow and F. R. de Boer, *Physics of Magnetism and Magnetic Materials*, 1st ed. (Kluwer Academic, New York, NY, 2004).

[2] I. Dzyaloshinsky, A thermodynamic theory of “weak” ferromagnetism of antiferromagnetics, J. Phys. Chem. Solids **4**, 241 (1958).

[3] T. Moriya, Anisotropic superexchange interaction and weak ferromagnetism, Phys. Rev. **120**, 91 (1960).

[4] N. Locatelli, V. Cros, and J. Grollier, Spin-torque building blocks, Nat. Mater. **13**, 11 (2014).

[5] S. Zuo, J. Liu, K. Qiao, Y. Zhang, J. Chen, N. Su, Y. Liu, J. Cao, T. Zhao, J. Wang, F. Hu, J. Sun, C. Jiang, and B. Shen, Spontaneous topological magnetic transitions in $NdCo_5$ rare-earth magnets, Adv. Mater. **33**, 2103751 (2021).

[6] V. Kisiček, D. Dominko, M. Čulo, Ž. Rapljenović, M. Kuveždić, M. Dragičević, H. Berger, X. Rocquefelte, M. Herak, and T. Ivek, Spin-reorientation-driven linear magnetoelectric effect in topological antiferromagnet Cu_3TeO_6, Phys. Rev. Lett. **132**, 096701 (2024).

[7] R. Pal, B. Pal, S. Mondal, R. O. Sharma, T. Das, P. Mandal, and A. N. Pal, Spin-reorientation driven emergent phases and unconventional magnetotransport in quasi-2D vdW ferromagnet Fe_4GeTe_2, npj 2D Mater. Appl. **8**, 30 (2024).

[8] M. T. Johnson, P. J. H. Bloemen, F. J. A. den Broeder, and J. J. de Vries, Magnetic anisotropy in metallic multilayers, Rep. Prog. Phys. **59**, 1409 (1996).

[9] R. L. White, Review of recent work on the magnetic and spectroscopic properties of the rare-earth orthoferrites, J. Appl. Phys. **40**, 1061 (1969).

[10] T. Yamaguchi, Theory of spin reorientation in rare-earth orthochromites and orthoferrites, J. Phys. Chem. Solids **35**, 479 (1974).

[11] P. A. Algarabel, A. del Moral, M. R. Ibarra, and J. I. Arnaudas, Spin reorientation in $RECo_5$ compounds: A.C. susceptibility and thermal expansion, J. Phys. Chem. Solids **49**, 213 (1988).

[12] Z. Huang, W. Wang, H. Ye, S. Bao, Y. Shangguan, J. Liao, S. Cao, R. Kajimoto, K. Ikeuchi, G. Deng, M. Smidman, Y. Song, S.-L. Yu, J.-X. Li, and J. Wen, Microscopic origin of the spin-reorientation transition in the kagome topological magnet $TbMn_6Sn_6$, Phys. Rev. B **109**, 014434 (2024).

[13] M. C. Weber, M. Guennou, D. M. Evans, C. Toulouse, A. Simonov, Y. Kholina, X. Ma, W. Ren, S. Cao, M. A. Carpenter, B. Dkhil, M. Fiebig, and J. Kreisel, Emerging spin–phonon coupling through cross-talk of two magnetic sublattices, Nat. Commun. **13**, 443 (2022).

[14] L. M. Levinson, M. Luban, and S. Shtrikman, Microscopic model for reorientation of the easy axis of magnetization, Phys. Rev. **187**, 715 (1969).

[15] K. P. Belov, A. K. Zvezdin, A. M. Kadomtseva, and R. Z. Levitin, Spin-reorientation transitions in rare-earth magnets, Sov. Phys.-Usp. **19**, 574 (1976).

[16] S. J. Yuan, Y. M. Cao, L. Li, T. F. Qi, S. X. Cao, J. C. Zhang, L. E. DeLong, and G. Cao, First-order spin reorientation transition and specific-heat anomaly in $CeFeO_3$, J. Appl. Phys. **114** (2013).

[17] Y. Song, J. Zhang, H. Li, H. Zhong, F. Long, Z. Wang, Y. Xu, X. Zheng, H. Zhang, Q. Huang, Y. Zhang, X. Xing, and J. Chen, Unusual magnetocaloric effect triggered by spin reorientation, Adv. Energy Mater.**14**, 2402527 (2024).

[18] J. Y. Law, V. Franco, L. M. Moreno-Ramírez, A. Conde, D. Y. Karpenkov, I. Radulov, K. P. Skokov, and O. Gutfleisch, A quantitative criterion for determining the order of magnetic phase transitions using the magnetocaloric effect, Nat. Commun. **9**, 2680 (2018).

[19] H. Horner and C. M. Varma, Nature of spin-reorientation transitions, Phys. Rev. Lett. **20**, 845 (1968).

[20] R. G. Moore, S. Okamoto, H. Li, W. R. Meier, H. Miao, H. N. Lee, M. Hashimoto, D. Lu, E. Dagotto, M. A. McGuire, and B. C. Sales, Topological electronic structure evolution with symmetry-breaking spin reorientation in $(Fe_{1-x}Co_x)Sn$, Phys. Rev. B **106**, 115141 (2022).

[21] K. Karube, L. Peng, J. Masell, M. Hemmida, H. Krug von Nidda, I. Kézsmárki, X. Yu, Y. Tokura, and Y. Taguchi, Doping control of magnetic anisotropy for stable antiskyrmion formation in schreibersite $(Fe, Ni)_3P$ with S_4 symmetry, Adv. Mater. **34**, 2108770 (2022).

[22] H. Masuda, H. Sakai, H. Takahashi, Y. Yamasaki, A. Nakao, T. Moyoshi, H. Nakao, Y. Murakami, T. Arima, and S. Ishiwata, Field-induced spin reorientation in the antiferromagnetic Dirac material $EuMnBi_2$ revealed by neutron and resonant x-ray diffraction, Phys. Rev. B **101**, 174411 (2020).

[23] S. Yamamoto, H. Suwa, T. Kihara, T. Nomura, Y. Kotani, T. Nakamura, Y. Skourski, S. Zherlitsyn, L. Prodan, V. Tsurkan, H. Nojiri, A. Loidl, and J. Wosnitza, Element-specific field-induced spin reorientation and tetracritical point in $MnCr_2S_4$, Phys. Rev. B **103**, L020408 (2021).

[24] L. Prodan, S. Yasin, A. Jesche, J. Deisenhofer, H.-A. Krug von Nidda, F. Mayr, S. Zherlitsyn, J. Wosnitza, A. Loidl, and V. Tsurkan, Unusual field-induced spin reorientation in $FeCr_2S_4$: Field tuning of the Jahn-Teller state, Phys. Rev. B **104**, L020410 (2021).

[25] Z. Lin, M. Lohmann, Z. A. Ali, C. Tang, J. Li, W. Xing, J. Zhong, S. Jia, W. Han, S. Coh, W. Beyermann, and J. Shi, Pressure-induced spin reorientation transition in layered ferromagnetic insulator $Cr_2Ge_2Te_6$, Phys. Rev. Mater. **2**, 051004(R) (2018).

[26] S. A. Skorobogatov, L. S. Wu, T. Xie, K. A. Shaykhutdinov, E. V. Pomjakushina, A. Podlesnyak, and S. E. Nikitin, Pressure control of the spin reorientation transition in the rare-earth orthoferrite $YbFeO_3$, Phys. Rev. B **108**, 054432 (2023).

[27] C. Bordel, J. Juraszek, D. W. Cooke, C. Baldasseroni, S. Mankovsky, J. Minár, H. Ebert, S. Moyerman, E. E. Fullerton, and F. Hellman, Fe spin reorientation across the metamagnetic transition in strained FeRh thin films, Phys. Rev. Lett. **109**, 117201 (2012).

[28] D. Kong, A. Kovács, M. Charilaou, M. Altthaler, L. Prodan, V. Tsuran, D. Meier, X. Han, I. Kézsmárki, and R. E. Dunin-Borkowski, Strain engineering of magnetic anisotropy in the kagome magnet Fe_3Sn_2, ACS Nano **19**, 8142 (2025).

[29] A. V. Kimel, A. Kirilyuk, A. Tsvetkov, R. V. Pisarev, and T. Rasing, Laser-induced ultrafast spin reorientation in the antiferromagnet $TmFeO_3$, Nature (London) **429**, 850 (2004).

[30] J. T. Weber, A. Kovács, M. Charilaou, D. Kong, L. Prodan, V. Tsurkan, A. Schröder, N. S. Kiselev, I. Kézsmárki, R. E. Dunin-Borkowski, A. H. Tavabi, and S. Schäfer, All-optical stochastic switching of magnetization textures in Fe_3Sn_2, arXiv:2503.05660.

[31] I. Kézsmárki, S. Bordács, P. Milde, E. Neuber, L. M. Eng, J. S. White, H. M. Rønnow, C. D. Dewhurst, M. Mochizuki, K.

Yanai, H. Nakamura, D. Ehlers, V. Tsurkan, and A. Loidl, Néel-type skyrmion lattice with confined orientation in the polar magnetic semiconductor GaV_4S_8, Nat. Mater. **14**, 1116 (2015).

[32] D. Ehlers, I. Stasinopoulos, V. Tsurkan, H.-A. Krug von Nidda, T. Fehér, A. Leonov, I. Kézsmárki, D. Grundler, and A. Loidl, Skyrmion dynamics under uniaxial anisotropy, Phys. Rev. B **94**, 014406 (2016).

[33] S. Bordács, A. Butykai, B. G. Szigeti, J. S. White, R. Cubitt, A. O. Leonov, S. Widmann, D. Ehlers, H.-A. K. von Nidda, V. Tsurkan, A. Loidl, and I. Kézsmárki, Equilibrium skyrmion lattice ground state in a polar easy-plane magnet, Sci. Rep. **7**, 7584 (2017).

[34] A. O. Leonov and I. Kézsmárki, Skyrmion robustness in non-centrosymmetric magnets with axial symmetry: The role of anisotropy and tilted magnetic fields, Phys. Rev. B **96**, 214413 (2017).

[35] M. Preißinger, K. Karube, D. Ehlers, B. Szigeti, H.-A. Krug von Nidda, J. S. White, V. Ukleev, H. M. Rønnow, Y. Tokunaga, A. Kikkawa, Y. Tokura, Y. Taguchi, and I. Kézsmárki, Vital role of magnetocrystalline anisotropy in cubic chiral skyrmion hosts, npj Quantum Mater. **6**, 65 (2021).

[36] O. Meshcheriakova, S. Chadov, A. K. Nayak, U. K. Rößler, J. Kübler, G. André, A. A. Tsirlin, J. Kiss, S. Hausdorf, A. Kalache, W. Schnelle, M. Nicklas, and C. Felser, Large noncollinearity and spin reorientation in the novel Mn_2RhSn Heusler magnet, Phys. Rev. Lett. **113**, 087203 (2014).

[37] A. S. Sukhanov, B. E. Zuniga Cespedes, P. Vir, A. S. Cameron, A. Heinemann, N. Martin, G. Chaboussant, V. Kumar, P. Milde, L. M. Eng, C. Felser, and D. S. Inosov, Anisotropic fractal magnetic domain pattern in bulk $Mn_{1.4}PtSn$, Phys. Rev. B **102**, 174447 (2020).

[38] Y. Xiao, F. J. Morvan, A. N. He, M. K. Wang, H. B. Luo, R. B. Jiao, W. X. Xia, G. P. Zhao, and J. P. Liu, Spin-reorientation transition induced magnetic skyrmion in $Nd_2Fe_{14}B$ magnet, Appl. Phys. Lett. **117**, 132402 (2020).

[39] S. Bera, S. K. Pradhan, M. S. Khan, R. Pal, B. Pal, S. Kalimuddin, A. Bera, B. Das, A. N. Pal, and M. Mondal, Unravelling the nature of spin reorientation transition in quasi-2D vdW magnetic material, Fe_4GeTe_2, J. Magn. Magn. Mater. **565**, 170257 (2023).

[40] S. Wang, Z. Wang, J. Jiang, Y. Zhang, R. Li, Y. Feng, P. Liu, Y. Lu, Z. Sheng, H. Du, N. Gao, and B. Xiang, Temperature-driven spin reorientation transition in van der Waals $Cr_{1.7}Te_2$ ferromagnet, Appl. Phys. Lett. **124**, 232401 (2024).

[41] D. C. Jones, S. Das, H. Bhandari, X. Liu, P. Siegfried, M. P. Ghimire, S. S. Tsirkin, I. I. Mazin, and N. J. Ghimire, Origin of spin reorientation and intrinsic anomalous Hall effect in the kagome ferrimagnet $TbMn_6Sn_6$, Phys. Rev. B **110**, 115134 (2024).

[42] B. Lv, R. Zhong, X. Luo, S. Ma, C. Chen, S. Wang, Q. Luo, F. Gao, C. Fang, and W. Ren, Anomalous Hall effect and topological Hall effect in Kagome lattice material $Yb_{0.90}Mn_6Ge_{3.25}Ga_{0.39}$ single crystal, Scr. Mater. **255**, 116345 (2025).

[43] V. Kumar, N. Kumar, M. Reehuis, J. Gayles, A. S. Sukhanov, A. Hoser, F. Damay, C. Shekhar, P. Adler, and C. Felser, Detection of antiskyrmions by topological Hall effect in Heusler compounds, Phys. Rev. B **101**, 014424 (2020).

[44] Y. He, J. Kroder, J. Gayles, C. Fu, Y. Pan, W. Schnelle, C. Felser, and G. H. Fecher, Large topological Hall effect in an easy-cone ferromagnet $(Cr_{0.9}B_{0.1})Te$, Appl. Phys. Lett. **117**, 052409 (2020).

[45] B. Malaman, B. Roques, A. Courtois, and J. Protas, Structure cristalline du stannure de fer Fe_3Sn_2, Acta Crystallogr., Sect. B **32**, 1348 (1976).

[46] B. Malaman, D. Fruchart, and G. L. Caer, Magnetic properties of Fe_3Sn_2. II. Neutron diffraction study (and Mossbauer effect), J. Phys. F **8**, 2389 (1978).

[47] G. L. Caer, B. Malaman, and B. Roques, Mossbauer effect study of Fe_3Sn_2, J. Phys. F **8**, 323 (1978).

[48] G. L. Caer, B. Malaman, L. Haggstrom, and T. Ericsson, Magnetic properties of Fe_3Sn_2. III. A ^{119}Sn Mossbauer study, J. Phys. F **9**, 1905 (1979).

[49] G. He, L. Peis, R. Stumberger, L. Prodan, V. Tsurkan, N. Unglert, L. Chioncel, I. Kézsmárki, and R. Hackl, Phonon anomalies associated with spin reorientation in the Kagome ferromagnet Fe_3Sn_2, Phys. Status Solidi (b) **259**, 2100169 (2021).

[50] L. Ye, M. Kang, J. Liu, F. von Cube, C. R. Wicker, T. Suzuki, C. Jozwiak, A. Bostwick, E. Rotenberg, D. C. Bell, L. Fu, R. Comin, and J. G. Checkelsky, Massive Dirac fermions in a ferromagnetic kagome metal, Nature (London) **555**, 638 (2018).

[51] A. Biswas, O. Iakutkina, Q. Wang, H. C. Lei, M. Dressel, and E. Uykur, Spin-reorientation-induced band gap in Fe_3Sn_2: Optical signatures of Weyl nodes, Phys. Rev. Lett. **125**, 076403 (2020).

[52] Z. Lin, J.-H. Choi, Q. Zhang, W. Qin, S. Yi, P. Wang, L. Li, Y. Wang, H. Zhang, Z. Sun, L. Wei, S. Zhang, T. Guo, Q. Lu, J.-H. Cho, C. Zeng, and Z. Zhang, Flatbands and emergent ferromagnetic ordering in Fe_3Sn_2 kagome lattices, Phys. Rev. Lett. **121**, 096401 (2018).

[53] F. Schilberth, N. Unglert, L. Prodan, F. Meggle, J. Ebad Allah, C. A. Kuntscher, A. A. Tsirlin, V. Tsurkan, J. Deisenhofer, L. Chioncel, I. Kézsmárki, and S. Bordács, Magneto-optical detection of topological contributions to the anomalous Hall effect in a kagome ferromagnet, Phys. Rev. B **106**, 144404 (2022).

[54] Q. Du, Z. Hu, M.-G. Han, F. Camino, Y. Zhu, and C. Petrovic, Topological Hall effect anisotropy in kagome bilayer metal Fe_3Sn_2, Phys. Rev. Lett. **129**, 236601 (2022).

[55] Z. Hou, W. Ren, B. Ding, G. Xu, Y. Wang, B. Yang, Q. Zhang, Y. Zhang, E. Liu, F. Xu, W. Wang, G. Wu, X. Zhang, B. Shen, and Z. Zhang, Observation of various and spontaneous magnetic skyrmionic bubbles at room temperature in a frustrated kagome magnet with uniaxial magnetic anisotropy, Adv. Mater. **30**, 1706306 (2018).

[56] M. Altthaler, E. Lysne, E. Roede, L. Prodan, V. Tsurkan, M. A. Kassem, H. Nakamura, S. Krohns, I. Kézsmárki, and D. Meier, Magnetic and geometric control of spin textures in the itinerant kagome magnet Fe_3Sn_2, Phys. Rev. Res. **3**, 043191 (2021).

[57] S. A. Ekahana, Y. Soh, A. Tamai, D. Gosálbez-Martínez, M. Yao, A. Hunter, W. Fan, Y. Wang, J. Li, A. Kleibert, C. A. F. Vaz, J. Ma, H. Lee, Y. Xiong, O. V. Yazyev, F. Baumberger, M. Shi, and G. Aeppli, Anomalous electrons in a metallic kagome ferromagnet, Nature (London) **627**, 67 (2024).

[58] M. V. Gonçalves-Faria, A. Pashkin, Q. Wang, H. C. Lei, S. Winnerl, A. A. Tsirlin, M. Helm, and E. Uykur, Coherent phonon and unconventional carriers in the magnetic kagome metal Fe_3Sn_2, npj Quantum Mater. **9**, 31 (2024).

[59] W. Zhang, T. C. Asmara, Y. Tseng, J. Li, Y. Xiong, Y. Wei, T. Yu, C. W. Galdino, Z. Zhang, K. Kummer, V. N. Strocov,

Y. Soh, T. Schmitt, and G. Aeppli, Spin waves and orbital contribution to ferromagnetism in a topological metal, Nat. Commun. **15**, 8905 (2024).
[60] L. Wang, J. Zhu, H. Chen, H. Wang, J. Liu, Y.-X. Huang, B. Jiang, J. Zhao, H. Shi, G. Tian, H. Wang, Y. Yao, D. Yu, Z. Wang, C. Xiao, S. A. Yang, and X. Wu, Orbital magneto-nonlinear anomalous Hall effect in kagome magnet Fe_3Sn_2, Phys. Rev. Lett. **132**, 106601 (2024).
[61] L. A. Fenner, A. A. Dee, and A. S. Wills, Non-collinearity and spin frustration in the itinerant kagome ferromagnet Fe_3Sn_2, J. Phys.: Condens. Matter **21**, 452202 (2009).
[62] B. Fayyazi, K. P. Skokov, T. Faske, I. Opahle, M. Duerrschnabel, T. Helbig, I. Soldatov, U. Rohrmann, L. Molina-Luna, K. Güth, H. Zhang, W. Donner, R. Schäfer, and O. Gutfleisch, Experimental and computational analysis of binary Fe-Sn ferromagnetic compounds, Acta Mater. **180**, 126 (2019).
[63] K. Heritage, B. Bryant, L. A. Fenner, A. S. Wills, G. Aeppli, and Y. Soh, Images of a first-order spin-reorientation phase transition in a metallic kagome ferromagnet, Adv. Funct. Mater. **30**, 1909163 (2020).
[64] P. Wu, J. Song, X. Yu, Y. Wang, K. Xia, B. Hong, L. Zu, Y. Du, P. Vallobra, F. Liu, S. Torii, T. Kamiyama, Y. Xiong, and W. Zhao, Evidence of spin reorientation and anharmonicity in kagome ferromagnet Fe_3Sn_2, Appl. Phys. Lett. **119**, 082401 (2021).
[65] C. Xie, Y. Deng, D. Zhang, J. Li, Y. Xiong, M. Ma, F. Ma, W. Tong, J. Wang, W. Meng, Y. Hou, Y. Han, Q. Feng, and Q. Lu, Real-space imaging of intrinsic symmetry-breaking spin textures in a kagome lattice, Adv. Sci. **11**, 2404088 (2024).
[66] Q. Wang, S. Sun, X. Zhang, F. Pang, and H. Lei, Anomalous Hall effect in a ferromagnetic Fe_3Sn_2 single crystal with a geometrically frustrated Fe bilayer kagome lattice, Phys. Rev. B **94**, 075135 (2016).
[67] N. Kumar, Y. Soh, Y. Wang, and Y. Xiong, Magnetotransport as a diagnostic of spin reorientation: Kagome ferromagnet as a case study, Phys. Rev. B **100**, 214420 (2019).
[68] Y. Li, Q. Wang, L. DeBeer-Schmitt, Z. Guguchia, R. D. Desautels, J.-X. Yin, Q. Du, W. Ren, X. Zhao, Z. Zhang, I. A. Zaliznyak, C. Petrovic, W. Yin, M. Z. Hasan, H. Lei, and J. M. Tranquada, Magnetic-field control of topological electronic response near room temperature in correlated kagome magnets, Phys. Rev. Lett. **123**, 196604 (2019).
[69] J.-X. Yin, S. S. Zhang, H. Li, K. Jiang, G. Chang, B. Zhang, B. Lian, C. Xiang, I. Belopolski, H. Zheng, T. A. Cochran, S.-Y. Xu, G. Bian, K. Liu, T.-R. Chang, H. Lin, Z.-Y. Lu, Z. Wang, S. Jia, W. Wang, and M. Z. Hasan, Giant and anisotropic many-body spin–orbit tunability in a strongly correlated kagome magnet, Nature (London) **562**, 91 (2018).
[70] H. Tanaka, Y. Fujisawa, K. Kuroda, R. Noguchi, S. Sakuragi, C. Bareille, B. Smith, C. Cacho, S. W. Jung, T. Muro, Y. Okada, and T. Kondo, Three-dimensional electronic structure in ferromagnetic Fe_3Sn_2 with breathing kagome bilayers, Phys. Rev. B **101**, 161114(R) (2020).
[71] N. Kumar, Y. Soh, Y. Wang, J. Li, and Y. Xiong, Tuning the electronic band structure in a kagome ferromagnetic metal via magnetization, Phys. Rev. B **106**, 045120 (2022).
[72] A. Fitch, C. Dejoie, E. Covacci, G. Confalonieri, O. Grendal, L. Claustre, P. Guillou, J. Kieffer, W. de Nolf, S. Petitdemange, M. Ruat, and Y. Watier, ID22–the high-resolution powder-diffraction beamline at ESRF, J. Synchrotron Radiat. **30**, 1003 (2023).
[73] A. A. Tsirlin, L. Prodan, and O. Grendal, High-resolution x-ray diffraction study of the kagome metal Fe_3Sn_2, European Synchrotron Radiation Facility (2022).
[74] V. Petříček, M. Dušek, and L. Palatinus, Crystallographic computing system JANA2006: General features, Z. Krist. **229**, 345 (2014).
[75] U. Stuhr, B. Roessli, S. Gvasaliya, H. M. Rønnow, U. Filges, D. Graf, A. Bollhalder, D. Hohl, R. Bürge, M. Schild, L. Holitzner, C. Kaegi, P. Keller, and T. Mühlebach, The thermal triple-axis-spectrometer EIGER at the continuous spallation source SINQ, Nucl. Instrum. Methods Phys. Res., Sect. A **853**, 16 (2017).
[76] O. Kazakova, R. Puttock, C. Barton, H. Corte-León, M. Jaafar, V. Neu, and A. Asenjo, Frontiers of magnetic force microscopy, J. Appl. Phys. **125**, 060901 (2019).
[77] Y. Song, Y. Hao, S. Wang, J. Zhang, Q. Huang, X. Xing, and J. Chen, Complicated magnetic structure and its strong correlation with the anomalous Hall effect in Mn_3Sn, Phys. Rev. B **101**, 144422 (2020).
[78] Z. Zhang, M. Zhao, L. Ma, G. Li, C. Zhen, D. Zhao, and D. Hou, Large topological Hall effect arising from spin reorientation in kagome magnet Fe_3Ge, arXiv:2403.17354.
[79] R. Pal, J. J. Abraham, A. Mistonov, S. Mishra, N. Stilkerich, S. Mondal, P. Mandal, A. N. Pal, J. Geck, B. Büchner, V. Kataev, and A. Alfonsov, Disentangling the unusual magnetic anisotropy of the near-room-temperature ferromagnet Fe_4GeTe_2, Adv. Funct. Mater. **34**, 2402551 (2024).
[80] Y. Song, Y. Qiao, Q. Huang, C. Wang, X. Liu, Q. Li, J. Chen, and X. Xing, Opposite thermal expansion in isostructural noncollinear antiferromagnetic compounds of Mn_3A (A = Ge and Sn), Chem. Mater. **30**, 6236 (2018).
[81] R. C. O'Handley, *Modern Magnetic Materials: Principles and Applications* (Wiley, New York, 1999), p. 184.
[82] B. D. Cullity and C. D. Graham, *Introduction to Magnetic Materials* (Wiley, New York, 2008).
[83] L. Prodan, D. M. Evans, S. M. Griffin, A. Östlin, M. Altthaler, E. Lysne, I. G. Filippova, S. Shova, L. Chioncel, V. Tsurkan, and I. Kézsmárki, Large ordered moment with strong easy-plane anisotropy and vortex-domain pattern in the kagome ferromagnet Fe_3Sn, Appl. Phys. Lett. **123**, 021901 (2023).
[84] W. Sucksmith and J. E. Thompson, The magnetic anisotropy of cobalt, Proc. R. Soc. London, Ser. A **225**, 362 (1954).
[85] L. D. Landau, E. M. Lifshitz, and L. P. Pitaevskii, *Electrodynamics of Continuous Media*, 2nd ed., Course of Theoretical Physics, Vol. 8 (Elsevier, Bristol, 2013), pp. 159–162.
[86] A. Hubert and R. Schäfer, *Magnetic Domains: The Analysis of Magnetic Microstructures*, corrected 3rd printing (Springer, Berlin, 2009), p. 378.
[87] Y. Chen, B. Lv, Y. Wu, Q. Hu, J. Li, Y. Wang, Y. Xiong, J. Gao, J. Tang, M. Tian, and H. Du, Effects of tilted magnetocrystalline anisotropy on magnetic domains in Fe_3Sn_2 thin plates, Phys. Rev. B **103**, 214435 (2021).
[88] L. Prodan, "Easy-cone state mediating the spin reorientation in topological kagome magnet Fe_3Sn_2 (2025)" [Data set], Zenodo, 10.5281/zenodo.15367272.